An update to this article is included at the end

Resource

Cell Reports

Quantification of Protein Levels in Single Living Cells

Graphical Abstract

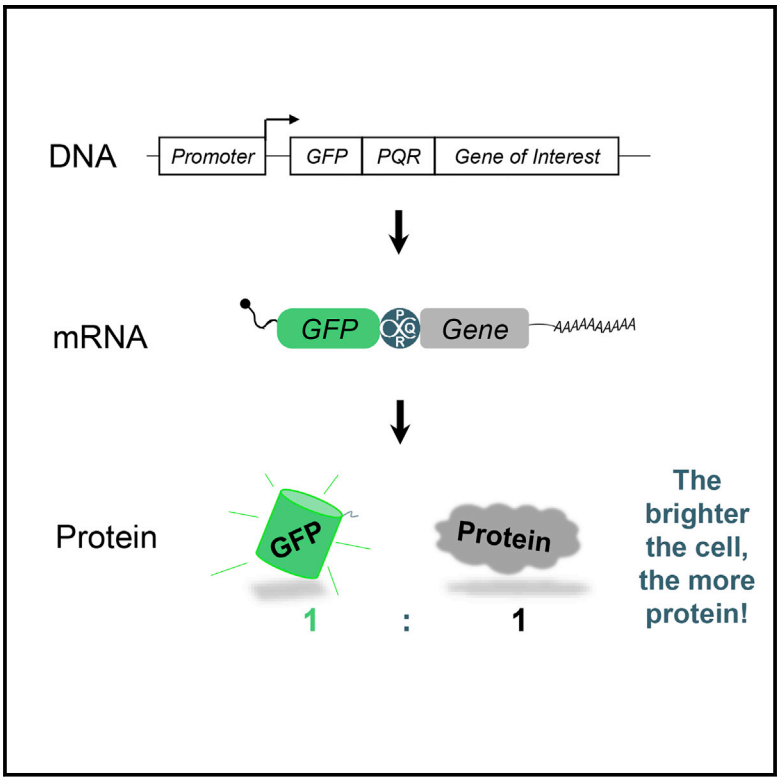

Authors

Chiu-An Lo, Ibrahim Kays, Farida Emran, Tsung-Jung Lin, Vedrana Cvetkovska, Brian Edwin Chen

Correspondence

brian.chen@mcgill.ca

In Brief

Lo et al. describe a technique called protein quantitation ratioing that allows for quantification of protein amounts in single cells in the living animal. The technique uses the fluorescence intensity of a reporter as a readout for the concentration of a protein within a cell.

Highlights

- Protein levels can be quantified using a fluorescent reporter
- Relative protein levels can be quantified in single living cells
- Genome editing allows for quantification of endogenous protein levels
- The PQR technique has broad possible applications

Lo et al., 2015, Cell Reports *13*, 2634–2644
December 22, 2015
http://dx.doi.org/10.1016/j.celrep.2015.11.048

CellPress

OPEN ACCESS
CellPress

Cell Reports
Resource

Quantification of Protein Levels in Single Living Cells

Chiu-An Lo,[1,3] Ibrahim Kays,[1,3] Farida Emran,[1] Tsung-Jung Lin,[1] Vedrana Cvetkovska,[1] and Brian Edwin Chen[1,2,*]
[1]Centre for Research in Neuroscience, Research Institute of the McGill University Health Centre, Montréal, QC H3G 1A4, Canada
[2]Departments of Medicine and Neurology and Neurosurgery, McGill University, Montréal, QC H3G 1A4, Canada
[3]Co-first author
*Correspondence: brian.chen@mcgill.ca
http://dx.doi.org/10.1016/j.celrep.2015.11.048

SUMMARY

Accurate measurement of the amount of specific protein a cell produces is important for investigating basic molecular processes. We have developed a technique that allows for quantitation of protein levels in single cells in vivo. This protein quantitation ratioing (PQR) technique uses a genetic tag that produces a stoichiometric ratio of a fluorescent protein reporter and the protein of interest during protein translation. The fluorescence intensity is proportional to the number of molecules produced of the protein of interest and is used to determine the relative amount of protein within the cell. We use PQR to quantify protein expression of different genes using quantitative imaging, electrophysiology, and phenotype. We use genome editing to insert *Protein Quantitation Reporters* into endogenous genomic loci in three different genomes for quantitation of endogenous protein levels. The PQR technique will allow for a wide range of quantitative experiments examining gene-to-phenotype relationships with greater accuracy.

INTRODUCTION

The most common methods for measuring absolute or relative protein amounts are protein assays and quantitative western blots or immunoblots, respectively (Bradford, 1976; Renart et al., 1979). All methods for protein quantitation start with the isolation of large quantities of the cell type of interest due to the limited sensitivity and detection capabilities of these techniques, making them time consuming and laborious (Walker, 2009). The cellular resolution of these techniques is also limited, because the isolated tissue is typically a heterogeneous population of cells that can include a wide range of cell types outside of a user's interest. These techniques are necessarily destructive processes, as cells must be lysed to extract their protein content for the detection processes (Walker, 2009). Inaccuracies in quantitation using immunodetection are further compounded by variability in the antibody used to detect the protein, such as the avidity and affinity of the antibody, access of the antibody to the protein epitope, phosphorylation state of the protein, and cross-reactivities of the antibody (Walker, 2009). The use of a "housekeeping" protein for normalization is subject to the same limitations, as housekeeping protein quantification is still dependent on antibody detection, and differences across conditions, along with cellular heterogeneity can increase or decrease the housekeeping protein quantified without affecting the protein of interest (e.g., epithelial cells within neural tissue may not express a neural protein), leading to an inaccurate ratio between the protein of interest and the normalization control.

We have developed a method to quantitate protein concentrations in single living cells using a fluorescent reporter (Figure 1). We modified and screened through RNA virus sequences that would allow for an equimolar separation of an upstream protein of interest and a downstream protein of interest, all contained within a single strand of RNA (de Felipe et al., 2006). Our logic was that when a fluorescent reporter is separated from the protein of interest, the number of fluorescent molecules produced is stoichiometric with the number of molecules of the protein of interest produced, and thus the fluorescence output can be used as a readout for the number of molecules of interest, i.e., its relative protein concentration (Figures 1A and 1B).

We initiated our screens using group IV, positive-sense, single-stranded RNA virus sequences encoding peptides called *cis*-acting hydrolase elements (CHYSELs). CHYSELs can interact with the ribosome during protein translation to produce non-canonical protein coding events and separate a nascent polypeptide chain from an actively translating sequence (Doronina et al., 2008). CHYSEL polypeptides (also known as "2A" and "2A-like" peptides, collectively) are used by RNA viruses to separate each of the viral genes to be translated (de Felipe et al., 2006). This allows for multiple proteins to be produced from the virus's single, polycistronic RNA strand. The mechanism by which separation of an upstream and downstream gene occurs is due to the specific sequence of CHYSEL residues upstream of a glycine proline separation point (Donnelly et al., 2001) (Figure 1A). In normal translation, the peptidyl transferase activity of the ribosome catalyzes the peptide bond of the growing peptide chain. The ribosome translocates and moves on to the next tRNA as the peptide chain is elongating through the exit tunnel (Fedyukina and Cavagnero, 2011). In the presence of the conserved CHYSEL residues that lie at the base of the exit tunnel, this forms a turn in the peptide chain that shifts the ester link between the peptide and the tRNA glycine away from the prolyl tRNA (Donnelly et al., 1997; Ryan et al., 2002). This torsion

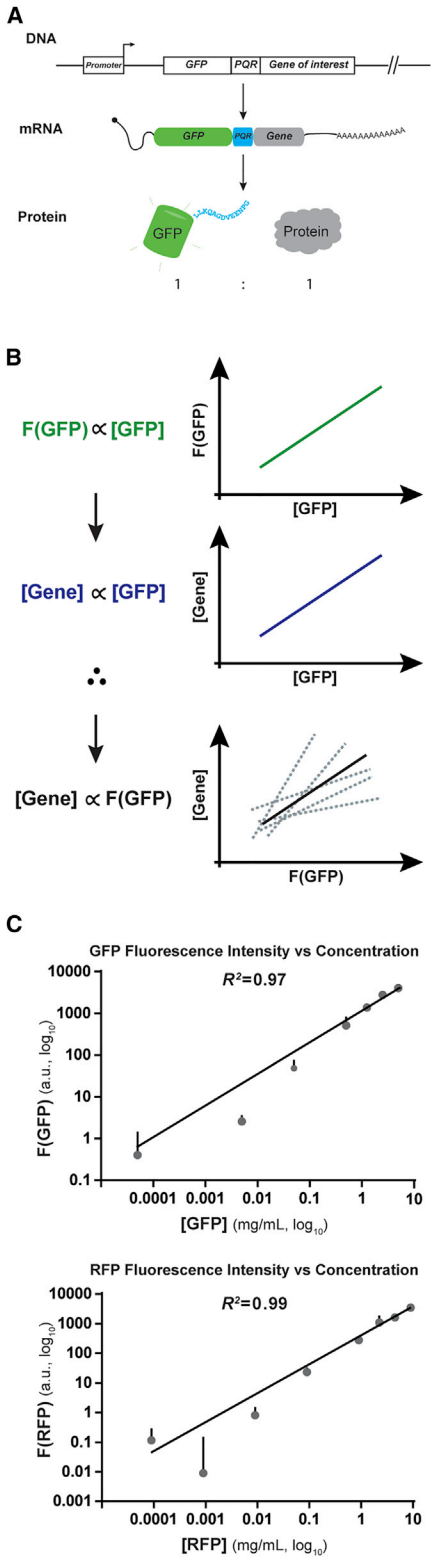

Figure 1. Protein Quantitation Ratioing Can Determine Relative Protein Concentration in Single Living Cells

(A) Stoichiometric protein translation can quantitate protein amounts. Insertion of a *Protein Quantitation Reporter* (*PQR*) between a fluorescent reporter (*GFP*) and a gene of interest creates a polycistronic mRNA for co-transcription and co-translation of GFP and the gene of interest. The *PQR* construct allows for one molecule of GFP to be synthesized for every one protein of interest synthesized. Because the fluorescence output of GFP is directly proportional to the concentration of GFP, the fluorescence intensity of a cell can be used to quantitate the concentration of the protein of interest.

(B) Linear relationships between fluorescence output, fluorescent protein concentration, and protein of interest concentration allow for protein quantitation ratioing. Because the fluorescence output of GFP is directly proportional to its concentration (top panel and C), then using a *PQR* will produce a stoichiometric ratio between GFP and the protein of interest (middle panel), therefore enabling the fluorescence intensity of GFP to be used as a measure of the protein of interest concentration (bottom panel). Any (linear) differences in post-translational processing, maturation, or insertion rates of the protein of interest or GFP will change the slope of the relationship (dotted gray lines). For example, if at steady state there are 11 functional molecules of a Shaker K^+ channel for every 41 functional molecules of GFP, then the relationship will still be linear. Importantly, protein concentration is predominantly controlled by translation, with very small contribution from protein stability and degradation.

(C) The fluorescence intensity of GFP and RFP is a linear function of its concentration over five orders of magnitude. Purified GFP (top panel) and RFP (bottom panel) were imaged using standard fluorescence microscopy. Pixel intensities are plotted in a.u. in $\log_{10}$. Coefficient of determination R^2 values from a simple linear regression model were calculated from the averages of five experiments. Error bars are SD.

causes the ribosome to stall and inhibits the peptidyl transferase activity, forcing the peptide chain to be released (Ryan et al., 2002). The ribosome skips the glycyl-prolyl peptide bond and re-initiates from the proline, and translation continues with the downstream protein.

To create a protein quantitation reporter, CHYSEL sequences must meet two important criteria. First, separation of the protein of interest and the reporter must be close to 100% reliable; otherwise, the resulting fusion product may interfere with protein function. Second, production of the fluorescent reporter must be stoichiometric with the protein of interest, since many CHYSELs produce inconsistent stoichiometric separations depending on cell state or cell type or at random. Although CHYSEL sequences have been shown to produce similar amounts of upstream and downstream proteins using high-throughput methods, these studies used CHYSEL peptides that do not consistently separate, and these fusion protein products contaminate the quantitation of protein concentration, because they are by definition equimolar (Figure 2) (Goedhart et al., 2011; Szymczak et al., 2004). Furthermore, we sought to create new CHYSEL sequences to exploit their usage to relate the linear dependence between fluorescent molecule concentration and its fluorescence output and fluorescent molecule concentration and the protein of interest concentration (Figures 1B and 1C). The production need not be equimolar at steady-state levels, but it should be consistently stoichiometric across cell states and types (Figure 1B).

RESULTS

We modified and tested different CHYSEL sequences for efficient and stoichiometric separation of the upstream and downstream genes and identified different sequences for use in *Drosophila* cells and vertebrate cells. We first screened for

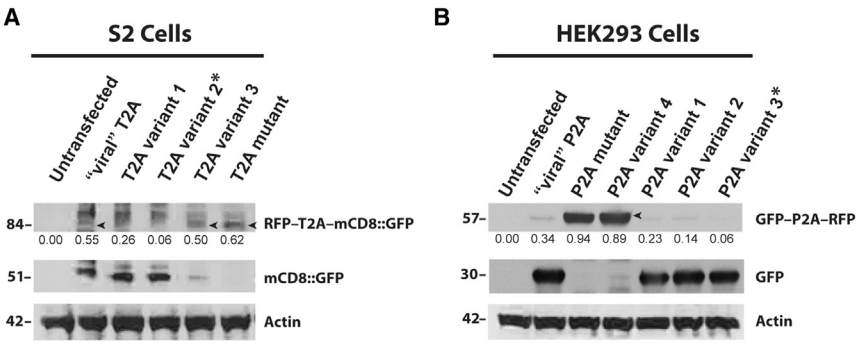

Figure 2. Wild-Type Viral CHYSEL Sequences Produce Unseparated Fusion Proteins, and *PQR* Sequences Produce Reliable Separation of Proteins

We modified and synthesized different viral CHYSEL sequences to screen for separation efficiency using immunoblots (representative examples shown) and stoichiometric production of proteins using quantitative imaging. Anti-GFP antibody was used to detect GFP (middle blots) versus fusion product of unseparated RFP and GFP (top blots). Anti-actin (bottom blots) was used to normalize pixel intensities of fusion product (numbers underneath top blots). We added glycine and serine N-terminal linkers to all synthesized CHYSEL sequences, for example on the 2A-like sequences from *Thosea asigna* virus (T2A) and to the 2A sequences from *Porcine teschovirus-1* (P2A).

(A) Wild-type T2A viral codon usage or codon optimization produces fusion protein production, whereas codon de-optimization enhances separation efficiency. Separation efficiency for each CHYSEL construct was tested using immunoblotting of RFP-CHYSEL-mCD8::GFP constructs transfected into *Drosophila* S2 cells for T2A-derived sequences. Manipulation of the T2A peptide sequence by adding glycine and serine linkers still produced a large fraction of fusion protein (arrowhead in lane 2, "viral" T2A). When we turned to manipulating codon sequence usage, we found that codon optimization produced equivalent or worse amounts of fusion products (arrowhead in lane 5, T2A variant 3, 100% codon optimized) compared to the viral CHYSEL sequence, along with diminished amounts of separated mCD8::GFP. Codon de-optimization of specific amino acids reduced the proportion of fusion product (lane 3, T2A variant 1 is 60% codon de-optimized and lane 4, T2A variant is 45% codon de-optimized). T2A variant 2, 45% codon de-optimization (asterisk), produced close to the background levels of the untransfected S2 cell lane. T2A mutant constructs (lane 6) that produced fusion products were used as positive controls.

(B) Codon de-optimization of specific CHYSEL residues produces reliable separation of proteins. We used HEK293 cells to test codon de-optimization of different CHYSEL residues using RFP-CHYSEL-GFP constructs derived from P2A sequences. We found that ~50% codon de-optimization of sequences (lane 6, P2A variant 3), without altering the final four codons, allows for greatest separation efficiency. P2A variant 4, with the last 4 codons de-optimized (lane 4) produced similar amounts of fusion product as the positive control (lane 3), with negligible amounts of unseparated GFP (middle blot). P2A variants 1, 2, and 3, changing 100%, 80%, and 50%, respectively, of the codons (except for the last 4 codons) produced decreasing amounts of fusion product and increasing amounts of separated GFP. All codon percentage change numbers do not include the glycine serine linker codons, which were required in all constructs (including "viral" sequences) to avoid large amounts of fusion products within the proteasome. Thus, using viral CHYSEL sequences will not work as *Protein Quantitation Reporters*, as these sequences leave a large fraction of uncleaved fusion protein product (arrowheads) that will contaminate any results of quantitation, and any experiments where fusion products are undesirable.

CHYSEL sequences that produce reliable separation of the upstream and downstream protein (Figure 2). We created different CHYSEL sequences for use in *Drosophila* and vertebrate cells, taken from different RNA viruses and modified, and then codon de-optimized at specific residues (Figure 2; Experimental Procedures). Thus, we collectively called these different DNA constructs for *Drosophila* and for vertebrate use *Protein Quantitation Reporters* (*PQRs*).

Next, we tested the stoichiometric ratio and linear relationship between different genes separated by our *PQRs* at the single-cell level. First, we quantified fluorescence intensities in HEK293 cells expressing a fusion protein of one molecule of GFP attached to one molecule of red fluorescent protein (RFP) by a mutated *PQR* linker (Figure 3). Because fluorescence intensity is directly proportional to the concentration of fluorescent molecules over several orders of magnitude, particularly at physiological concentrations (mg/ml) (Furtado and Henry, 2002) (Figure 1C), we measured the fluorescence output (i.e., brightness) of a cell to quantitate the ratio of GFP to RFP molecules. We found that green and red fluorescence intensities in cells expressing GFP::RFP were linearly correlated with a coefficient of determination R^2 = 0.74 (n = 74 cells, p < 0.001) (Figure 3A). Co-transfection of *GFP* and *RFP* into cells produced green and red fluorescence intensities that had a weak covariance, with R^2 = 0.37 (n = 59 cells, p < 0.001), due to differences in uptake, gene expression, and protein expression of *GFP*- versus *RFP*-encoding plasmids (Figure 3B). Co-transfection of plasmids is a common technique used for qualitative determination of protein co-expression, where the amount of DNA for each plasmid is titrated to a desired expression level, and it is then incorrectly assumed that the brightness of the cell corresponds to the expression level of the co-transfected plasmid(s) (Figure 3B). When we expressed GFP and RFP separated by a *PQR* sequence in cells, we found that the green and red fluorescence intensities were correlated with an R^2 = 0.78 and 0.66 for *GFP-PQR-RFP* (n = 77 cells, p < 0.001) and *RFP-PQR-GFP* (n = 77 cells, p < 0.001), respectively (Figures 3C and 3D). These R^2 values for *PQR* constructs were within the 95% confidence interval for the R^2 value for the GFP::RFP fusion protein, whereas the co-transfection of *GFP* and *RFP* R^2 value was outside the 95% confidence interval (Experimental Procedures; Figure S1). These results demonstrate that a *PQR* can produce stoichiometric ratios of proteins indistinguishable from fusing a fluorescent reporter. These *PQR* results were also not due to the incomplete separation of the upstream and downstream proteins, creating a subpopulation of GFP and RFP fusion product (Figure 2). To further determine whether genes separated by a *PQR* produced spatially separated proteins, we expressed spectrally distinct fluorophores with different subcellular localization signals, each separated by a *PQR* sequence in a single, polycistronic strand (YFP_{mito}–*PQR*–CFP_{nls}–*PQR*–*RFP*; Figures S2A–S2C). Fluorescence intensities of different colors in mitochondrial, nuclear, or cytoplasmic compartments were linearly correlated (ranging from R^2 = 0.54 to 0.69 for different organelles, n = 40 cells, p < 0.001), and intensities for the non-expected fluorophores were not detectable above background, confirming that fusion

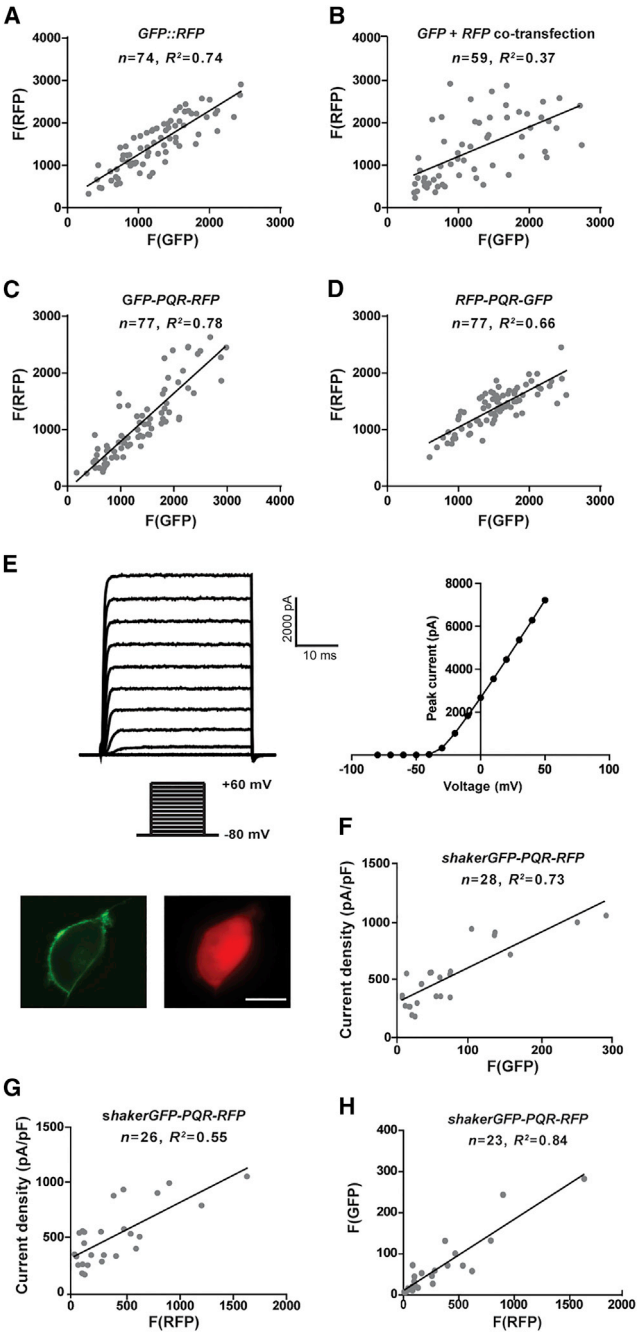

Figure 3. *Protein Quantitation Reporters* Can Correlate Fluorescence Intensity with Protein Amount

(A) Red and green fluorescence intensities of HEK293 cells expressing a fusion protein of GFP and RFP (GFP::RFP) were linearly correlated with a coefficient of determination, $R^2 = 0.74$ (n = 74 cells, $p < 0.001$). Fluorescence values are in a.u.

(B) Co-transfection of GFP and RFP produced a weak correlation between fluorescence intensities (n = 59 cells, $p < 0.001$).

(C and D) Insertion of a *PQR* between GFP and RFP produces red and green fluorescence intensities that were linearly correlated. R^2 values for *GFP-PQR-RFP* (c) and *RFP-PQR-GFP* (d) (n = 77 cells for both) were not significantly different from the fusion protein data ($p > 0.05$).

(E and F) K^+ channel current density was linearly correlated with green fluorescence intensity in cells expressing the Shaker K^+ channel fused to GFP, with a coefficient of determination $R^2 = 0.73$ (n = 28 cells, $p < 0.001$). Whole-cell patch-clamp recordings were performed on HEK293 cells, and voltage steps of +10 mV were given to generate an I-V curve (E). Steady-state current was measured at +30 mV and current density (pA/pF) was calculated using the membrane capacitance. Scale bar, 25 μm.

(G and H) Red fluorescence intensities were correlated with K^+ channel current density and green fluorescence in cells expressing *ShakerGFP-PQR-RFP*. R^2 values for current density to RFP, and GFP to RFP, were not significantly different from the current density to GFP positive control data ($p > 0.05$); see also Figures S1 and S3. These correlations were not due to unseparated RFP fusion products, since green fluorescence was restricted to the membrane and red fluorescence remained cytoplasmic (images in E). All fluorescence intensities are plotted in a.u.

proteins were not formed and localized to inappropriate cellular compartments. This also demonstrates that stoichiometric production of proteins is maintained for polycistronic mRNAs using *PQRs*, allowing for protein quantification in multiple regions of interest using different subcellular localization signals.

PQR Can Relate Cellular Phenotype as a Function of Protein Concentration

To determine whether *PQR* fluorescence intensity could correlate with a cellular phenotype directly related to protein concentration, we measured ion channel concentrations using whole cell patch clamp electrophysiology. We expressed the *Drosophila* Shaker potassium channel with a GFP molecule embedded within the inactivation domain (Batulan et al., 2010) separated by *PQR-RFP* (*ShakerGFP-PQR-RFP*) in HEK293 cells (Figure 3E). Measurements of K^+ channel current density compared to green fluorescence intensity of the cell membrane produced a linear correlation of $R^2 = 0.73$ (n = 28 cells, $p < 0.001$) (Figure 3F). Current density as a function of red fluorescence intensity had a correlation of $R^2 = 0.55$ ($p < 0.001$), and green to red fluorescence correlation was $R^2 = 0.84$ ($p < 0.001$) (Figures 3G and 3H), indicating that the steady-state ratio between RFP and a membrane protein four times larger and with several fold slower turnover maintained a linear relationship across expression ranges (coefficient of variation for current was 0.34) (Corish and Tyler-Smith, 1999; Zhao et al., 1995). We performed these electrophysiological and image analyses using different fluorescence microscopy methods and found strong linear correlations among all excitation methods (e.g., metal-halide lamp, mercury vapor lamp, lasers), fluorophores, and microscopy methods tested (ranging from R^2 = 0.90 to 0.94 between different methods) (Figure S2D). This is expected, because the linear relationship between concentration of a fluorophore and its brightness (Figure 1c) will be maintained regardless of excitation source, fluorophore, or emission detection method. This demonstrates that all standard fluorescence microscopy methods can be used with this technique.

To demonstrate the applicability of this technique in single neurons in animals, we used the predictable and quantitative changes in protein amounts that occur in the circadian system (Figure 4A). The transcription factor Period, or PER, controls the circadian rhythms of the *Drosophila* brain, and PER protein levels cycle every 24 hr as it is synthesized, shuttled into and out of the nucleus, and degraded in the proteasome (Hardin et al., 1990). To measure cyclic changes in fluorescence

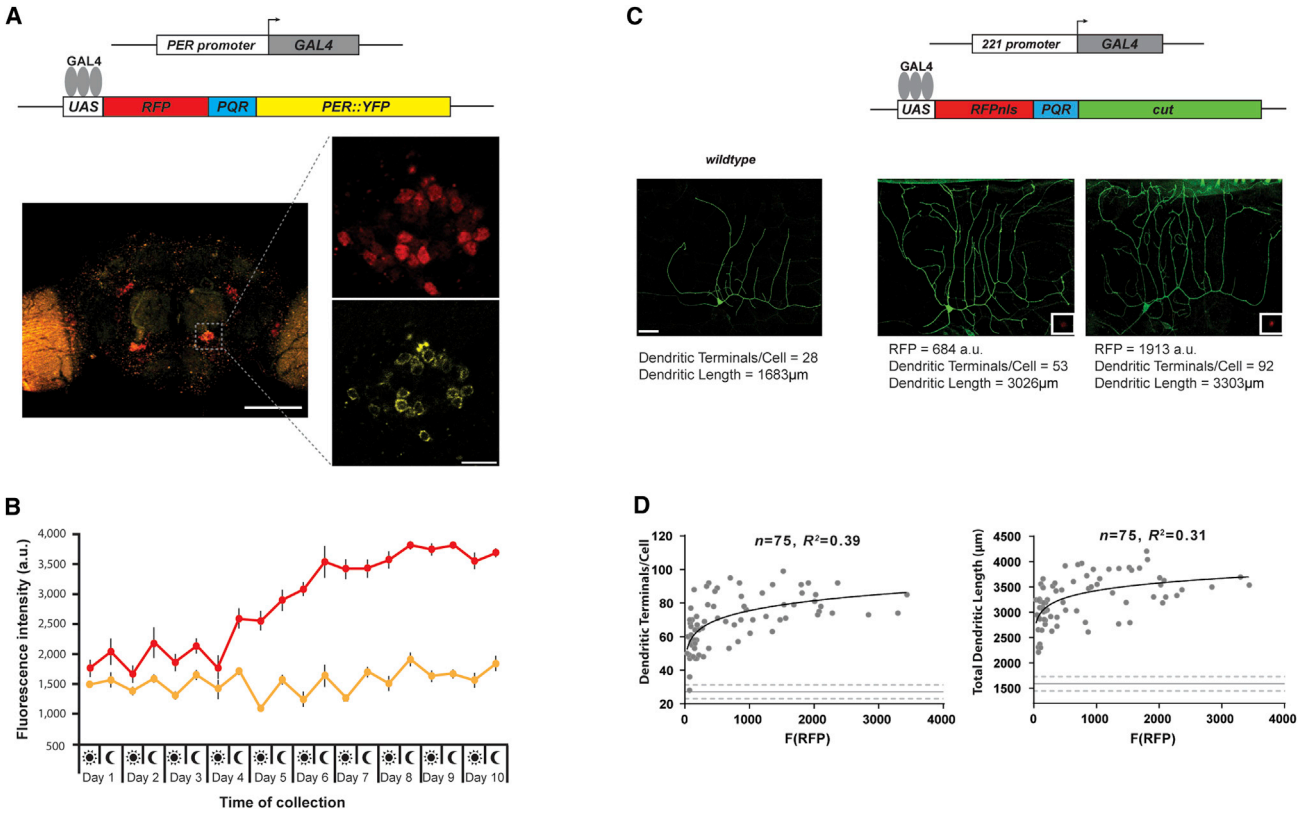

Figure 4. PQR Can Relate Cellular Phenotype as a Function of Protein Concentration

(A) PQR can detect cyclic increases in protein concentration over time. *RFP-PQR-PER::YFP* was used to quantitate changes in PER transcription factor levels in single neurons in the animal. An image of the *Drosophila* brain is shown with RFP and PER::YFP expression restricted to the small lateral ventral neurons (dotted box and right panels) using *Per-Gal4* to drive *UAS–RFP-PQR-PER::YFP*. Red fluorescence within the neurons remained in the cytoplasm, and yellow fluorescence was peri-nuclear. Scale bars are 100 μm (left panel) and 10 μm (right panels).

(B) Red fluorescence increased cyclically in neurons over timescales of days. Flies were entrained on a 12-hr light/dark cycle and red and yellow fluorescence intensities were measured within single neurons at zeitgeber time 0 (sun symbol) and 12 (moon symbol) (n = 6 cells/6 animals per time point). Yellow fluorescence intensities cycled every 24 hr without accumulating beyond a fixed value, reflecting the rapid lifetime of PER. Red fluorescence intensities were also cyclical but gradually increased over several days, reflecting the integrated amount of PER produced over time. Error bars are SEM. See also Figure S4.

(C) PQR in single living neurons is used to quantitatively relate dendritic complexity with Cut protein levels. Dendritic complexity of *Drosophila* da neurons is regulated by the transcription factor Cut. Wild-type class I da neurons (left panel) have relatively simple dendritic arbors. Expression of RFP_{nls}*-PQR-cut* within class I neurons increases dendritic branch number and total dendritic branch length (middle and right panels). Red fluorescence within the nucleus (inset in middle and right panels) reflecting Cut protein levels indicates that Cut controls dendritic growth in a concentration dependent manner. Posterior is up and dorsal to the right in all three panels. Scale bar, 30 μm.

(D) Dendritic complexity is logarithmically dependent on Cut protein concentration. The average number of dendritic branch terminals and total dendritic length in wild-type neurons is indicated by the solid gray lines (±1 SD, dashed lines) in the left and right panel, respectively.

intensity in single cells, we used a fusion protein of PER and yellow fluorescent protein (PER::YFP) separated by *PQR* with RFP. We used *period-Gal4* to drive expression of the *UAS–PER::YFP-PQR-RFP* construct within small lateral ventral neurons of the *Drosophila* brain (Figure 4A). We found that yellow fluorescence intensities cycled with a 24-hr periodicity without increasing beyond a fixed point, as the PER::YFP fusion protein was continually formed and destroyed (Figure 4B). RFP has a slightly longer half-life (26 hr) than PER (Corish and Tyler-Smith, 1999; Khmelinskii et al., 2012); thus, as RFP was co-translated and separated from the PER::YFP, we observed parallel production and degradation at early time points. However, the red fluorescence intensities eventually increased cyclically over several days until it saturated the fixed acquisition settings, set at the initially low red fluorescence intensities (Figure 4B).

We next used PQR to determine a quantitative relationship between protein amount and cellular phenotype in single living cells. *Drosophila* dendritic arborization (da) neurons can be classified into four groups (class I, II, III, and IV) based on their dendritic arbor complexity, and the transcription factor Cut has been implicated in regulating this complexity in a dosage-dependent manner (Grueber et al., 2003). However, it is not clear how Cut protein levels regulate neurite outgrowth. For example, the transcription factor may act as a binary switch or have a linear relationship with dendritic growth. Because da neurons are relatively large cells (Figure 4C) and we surmised that as a transcription factor, low levels of Cut would produce significant phenotypes,

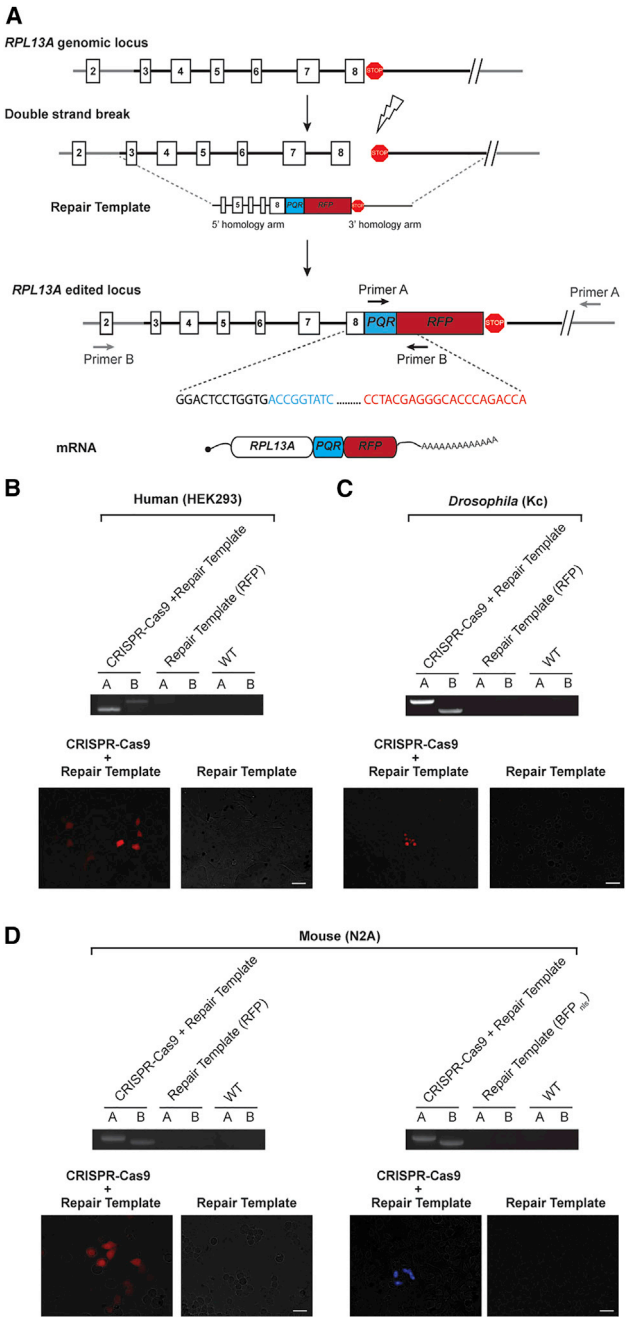

Figure 5. *PQRs* Can Be Inserted into Any Genomic Locus to Quantitate Endogenous Protein Levels

(A) Insertion of a *PQR* before the final stop codon of the endogenous gene maintains the mRNA production fidelity and the 3′ UTR for all isoforms of the mRNA with the *PQR*. A site-specific DNA double-strand break is created using the CRISPR-Cas9 system. The break is repaired by the cell using homologous recombination, and in the presence of an exogenous repair template with appropriate homology arms, the locus is replaced with the *PQR* edited version. Colored nucleotide sequences represent genomic sequencing results of an edited mouse *Rpl13a* gene with a *PQR-RFP* insertion.

(B–D) Targeted genome editing allows for insertion of a *PQR* into genes in different genomes. Different repair templates and guide RNAs for CRISPR-Cas9 were designed for the *RPL13A* gene in human (B), *Drosophila* (C), and mouse (D) genomes. Edited *RPL13A* genes with *PQR* produced RFP or BFP with a nuclear localization signal (BFP_{nls}). *PQR* insertion was verified using genomic PCR genotyping with primer pairs (A and B) that spanned *PQR* and outside the homology arms, followed by genomic sequencing. Scale bars, 100 μm.

we used a *PQR* with a nuclear localization signal (RFP_{nls}) to sequester the fluorophore and enhance the signal. We selectively expressed *UAS-RFP_{nls}-PQR-cut* in class I da neurons using the *221-Gal4, UAS-mCD8::GFP* line. We measured red fluorescence within the nucleus and used GFP to image the dendritic morphology to quantify the total dendritic arbor length and number of terminal branches (Figure 4C). We found that dendritic arbor complexity (number of dendritic terminals or total dendritic length) increases logarithmically with Cut protein levels until the dendritic branching effect was saturated (Figure 4D). These results indicate that Cut regulates dendritic arbor complexity in a concentration-dependent non-linear manner.

Can *PQRs* quantify endogenous protein levels? We next sought to insert *PQRs* into endogenous genomic loci to create a polycistronic mRNA that would preserve regulatory elements, such as the mRNA UTRs (Figure 5A). We used clustered regularly interspaced short palindromic repeats/Cas9 (CRISPR-Cas9) genome editing to generate custom RNAs that guide Cas9 nuclease to create a double-strand break at a specific genomic locus (Jinek et al., 2012). DNA double-strand breaks within a cell can be repaired through homologous recombination, and in the presence of an exogenous repair template containing DNA sequences of interest flanked by homologous sequence arms, foreign sequences can be recombined into the genome (Gaj et al., 2013). We generated repair templates to insert a *PQR* after the protein coding sequence of a gene, but before the final stop codon and 3′ UTR, to produce a single RNA strand encoding the endogenous protein of interest and a fluorescent reporter (Figure 5A). We inserted *PQRs* with RFP or blue fluorescent protein with a nuclear localization signal (BFP_{nls}) within the endogenous *RPL13A* genomic locus in human, *Drosophila*, and mouse genomes using HEK293, Kc, and Neuroblastoma-2A cells, respectively (Figures 5B–5D).

Using these genome-edited cells, we then wanted to examine the relationship between absolute mRNA transcript numbers and protein amount in the same cell. We combined PQR of endogenous protein production with single cell qPCR (Figure 6). We first imaged a live cell expressing a *PQR* and then lysed the cell to extract and measure its *PQR* mRNA transcripts (Figure 6A). Using our HEK293 cell line carrying a *PQR-RFP* reporter at the endogenous *RPL13A* locus (Figure 5B), we found that the number of mRNA molecules ranged from 50 to 570, and RPL13A relative protein amounts as measured by RFP fluorescence intensity, clustered between 200 and 800 a.u., resulting in no correlation between *RPL13A* mRNA versus protein amounts (R^2 = 0.03; n = 22) (Figures 6B–6D). As a comparison, we inserted a *PQR-GFP* reporter into the immunoglobulin kappa (κ) light chain genomic locus, *IgK*, in the mouse monoclonal antibody cell line, 22c10 (Figure 6E) (Fujita et al., 1982). As expected, these 22c10 cells produced a large amount of *IgK* mRNA ranging from 1,500 to 180,500 molecules in a single cell, despite being derived from a single clonal cell (Figures 6F and 6G). The green fluorescence

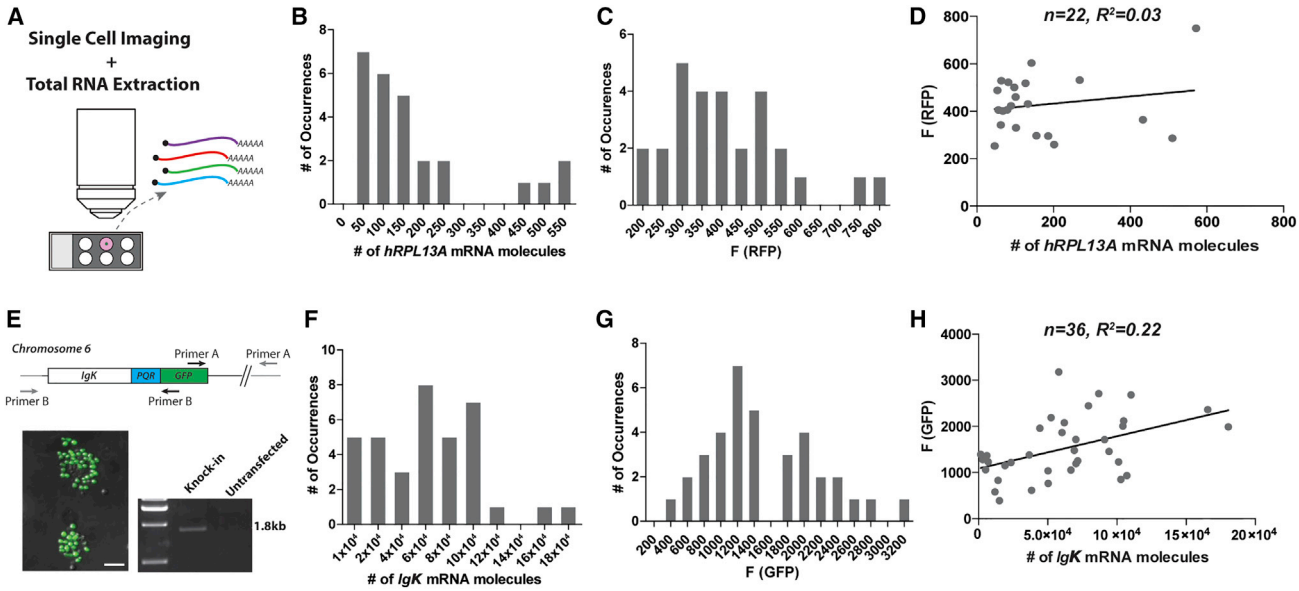

Figure 6. RNA and Protein Quantification in Single Cells

(A) Fluorescence intensity of single cells with a PQR knockin is measured and cells are then lysed for total RNA extraction and single-cell qPCR.

(B) Frequency distribution of *RPL13A* mRNA amounts measured from single HEK293 cells shows moderate expression of the *RPL13A* gene. qPCR of *RPL13A* mRNA specifically containing *PQR* constructs was performed to avoid variability due to heterozygosity or polyploidy of the cells.

(C and D) RFP fluorescence intensities (in a.u.) from single *RPL13A-PQR-RFP* knockin cells shows a moderate distribution but had a weak linear correlation to mRNA amounts.

(E) The endogenous immunoglobulin kappa light chain (*IgK*) locus is edited to insert a *PQR-GFP* reporter at the end of the constant region in 22c10 mouse hybridoma cells. The correct insertion is verified by PCR primer pairs that lie within and outside of the locus (arrows). 22c10 hybridoma cells produce green fluorescence after insertion of a *PQR-GFP* into the endogenous *IgK* locus. Scale bar, 25 μm. Representative PCR genotyping results show the expected size in the CRISPR-Cas9 transfected cells.

(F–H) Frequency distributions of *IgK* mRNA amounts and PQR-GFP fluorescence intensities measured from single 22c10 cells show the broad range and high levels of mRNA and protein expression. The IgK protein expression was not strongly correlated with its mRNA amounts; see also Figure S3.

intensity distribution also varied widely, which produced a weak correlation between *IgK* transcript number and IGK protein amount (R^2 = 0.22, n = 36) (Figure 6H). To confirm that our fluorescence intensity distributions and correlations were not due to differences between the fluorophores, cell types, or procedure, we first swapped the *PQR* fluorophores from the *Rpl13a* and *IgK* genes to create *Rpl13a-PQR-GFP*$_{nls}$ and *IgK-PQR-RFP*. Next, we used CRISPR-Cas9 genome editing on both of these genes within a single cell line to create double-knockin cells (Figure S3). By measuring green fluorescence in the nucleus and red fluorescence in the cytoplasm within a single 22c10 cell and then quantifying its *Rpl13a* and *IgK* mRNA amounts, we verified that the mRNA expression of these genes is a poor predictor of actual protein translation. These results using both mouse and human genes confirm previous studies demonstrating the poor correspondence between mRNA expression and actual protein production (Schwanhäusser et al., 2011; Shalek et al., 2013; Vogel and Marcotte, 2012).

DISCUSSION

The technique we describe here, protein quantitation ratioing, uses standard fluorescence imaging available through multiple microscopy methods. PQR is fast, has sensitivity at single-cell resolution, and can be performed with time lapse in living cells. Using a cell's brightness as a readout for the protein expression level of a gene, PQR can have a wide range of applications in cell biology to quantitatively measure relationships between phenotypes and protein levels.

The PQR technique quantifies steady-state protein levels within a cell, and differences in kinetics of the upstream and downstream proteins (e.g., folding, maturation, or turnover rates) will change the slope of the linear relationship, but the fluorescence will still be proportional to the number of molecules translated (Figure 1B). For example, the *Drosophila* Shaker K^+ channel is homo-tetrameric (i.e., four molecules are required for a single functional channel) and has a turnover rate of several days but has complex and comparatively rapid internalization and insertion rates on timescales of minutes to hours (de Souza and Simon, 2002; Jugloff et al., 2000; Zhao et al., 1995). Our PQR results using the Shaker K^+ channel demonstrate that the technique can be used even for complicated membrane proteins with slow degradation rates. In addition, protein concentration is predominantly controlled by translation, with very small contribution (<5%) from protein stability and degradation (Schwanhäusser et al., 2011). To model how differences in protein dynamics might affect PQR measurements, we simulated two cells expressing *PQRs* that exhibited different kinetics of a protein of interest (Figure S4A). We found that differences in protein turnover did not adversely affect PQR accuracy, with >85% of

cases producing at least 90% accurate quantification, across tens of thousands of proteins with randomly varying kinetics (Figure S4). This is because PQR measurements are ratiometric between two cells rather than absolute measurements of protein abundance, and because the CHYSEL mechanism forces not only the identical "on" rate of the protein of interest, but also the exact protein amount being produced. This creates a regularly resetting mechanism for the PQR fluorophore to match the protein of interest kinetics. Experimentally, we used the circadian system as an extreme example of very tightly regulated gene expression, with precisely controlled mRNA production and mRNA degradation, and protein production and degradation (Hardin et al., 1990). Our PQR measurements could integrate the cyclic production of PER protein until the PQR fluorescence intensities saturated (Figure 4B). However, cyclic changes in PER protein can still be accurately measured at any arbitrary later time point by resetting the acquisition setting for PQR fluorescence (Figure S4C), demonstrating the robust sensitivity of the PQR technique. More precise spatial and temporal measurements of protein kinetics may be obtained through the use of photoswitchable molecules to allow for subcellular activation and quantitative imaging of newly synthesized fluorescent molecules. Although the PQR technique quantifies protein amounts indirectly, it is a similarly indirect measurement as quantitative immunoblots and qPCR. Currently, the only alternatives to PQR are quantitative immunoblots and protein assays, which require isolation of large amounts of heterogeneous starting material.

For our positive controls, we fused a fluorescent protein to a protein of interest to track and quantitate protein amounts. Fusion proteins, howeer, can be undesirable to biologists. A fusion protein must be expressed at high enough levels to detect and be accessible for analysis (e.g., it may be membrane associated or secreted), and any modification can interfere with protein stability, activity, or function (e.g., N-terminal and C-terminal additions can affect type I and type II transmembrane proteins or alter intracellular signaling). Unlike a physical tag, PQR uses a genetic tag separated during protein synthesis, leaving only ~20 amino acids on the carboxy terminus of the upstream protein and a single proline at the start of the downstream protein. Using the integral membrane protein Shaker K^+ channel, we verified that placement of the *Shaker* gene upstream or downstream of the *PQR* sequences did not affect its membrane insertion or properties (Figure S2E). Separation of the *PQR* to different locations than the protein of interest allows for easier quantification of genes expressed at low levels (Figure 4C), where the PQR can be sequestered within the nucleus or nucleolus (Tsai et al., 2008), or for large or complex cells such as neurons (Figure 4C), or for quantification of transmembrane and secreted proteins, such as the production of antibodies. For example, the genomic organization of vertebrate antibodies joins upstream variable exons to a final 3′ constant exon (Hsu et al., 2006), and insertion of a *PQR* between the coding sequence and the 3′ UTR will allow for quantification of antibody production in all cells that synthesize the specific antibody type.

The *RPL13A* gene encodes for Ribosomal Protein L13A and is expressed in every cell in all eukaryotes at moderately high levels (Figure 6B), and it is commonly used as a housekeeping gene for normalization in quantitative DNA and protein measurements (Mane et al., 2008). Therefore, quantitation of endogenous RPL13A protein levels in single cells can be used as a measure of an individual cell's overall transcriptional and translational status (Figures 5 and 6). Quantifying RPL13A fluorescence levels in a second channel (e.g., RFP or BFP_{nls}) allows for normalization across cells or experiments and for optical effects such as spherical aberration, optical distortions, and imaging depths during in vivo imaging. Thus, using this approach, the relative levels of any protein of interest can be determined across conditions using the ratio of fluorescence between the protein of interest normalized to RPL13A fluorescence.

Quantification of endogenous proteins using PQR does not necessarily require the generation of knockin organisms. For example, efficient genome editing of post-mitotic neurons transfected with the CRISPR-Cas9 system has been demonstrated using biolistic transfection and in utero electroporation (Straub et al., 2014). This will allow for PQR of endogenous proteins within specific cells in vivo, for example by transfection of CRISPR-Cas9 for homologous recombination of *PQR* constructs within neurons. The protein quantitation ratioing technique has broad expansion possibilities, such as measuring protein production in single cells over time for drug screening, quantitation of endogenous protein levels in single cells in vivo, normalization across experiments and optical effects using the ratio of RPL13A levels, and allowing a wide range of quantitative experiments examining gene to phenotype relationships.

EXPERIMENTAL PROCEDURES

Protein Quantitation Reporter Constructs

Sequences for CHYSEL peptides were tested from group IV, positive-sense single-stranded RNA viruses, including the Picornaviridae family for 2A peptides or the Permutotetraviridae family for 2A-like peptides (Diao and White, 2012; Kim et al., 2011). For our initial screens, we mostly focused on four broad CHYSEL peptide sequences from *Equine rhinitis A* virus (E2A), *Foot-and-mouth disease* virus (F2A), *Porcine teschovirus-1* (P2A), and *Thosea asigna* virus (T2A) and tested for stoichiometric production and separation of fluorescent proteins and Shaker potassium channel. We added glycine and serine linkers to the N terminus of all CHYSEL sequences tested to enhance peptide separation (Yang et al., 2008). We selected the amino acid sequence ATNFSLLKQAGDVEENPGP from the porcine teschovirus-1 for use in mammalian cells (Kim et al., 2011) and EGRGSLLTCGDVEENPGP from the *Thosea asigna* insect virus for use in *Drosophila* cells (Diao and White, 2012). We compared codon optimization of the CHYSEL peptides versus the viral sequences of the CHYSEL peptides, and we found that both the original viral sequence and the codon-optimized forms resulted in a large fraction of unseparated, fusion product (Figures 2 and S5). Codon optimization often created a larger proportion of unseparated product, indicating that codon optimization could be worse for protein quantitation. Thus, we surmised that codon optimization could speed up ribosomal activity, causing it to ignore the separation event between the final glycine and proline of the CHYSEL peptide. We tested DNA sequences that were selected for nonfavored codons to decrease translation speed, which we found to enhance reliable separation (Figures 2 and S5) (Novoa and Ribas de Pouplana, 2012; Zhou et al., 2011). The DNA sequence chosen for the *PQR* in mammalian cells (P2A-derived with glycine and serine linker, codon variation 3) was 5′-GGAAGCGGAGCGACGAATTTTA GTCTACTGAAACAAGCGGGAGACGTGGAGGAAAACCCTGGACCT-3′. The DNA sequence chosen for the *PQR* in *Drosophila* cells (T2A-derived with glycine and serine linker, codon variation 2) was 5′-GGAAGCGGAGAAGGT CGTGGTAGTCTACTAACGTGTGGTGACGTCGAGGAAAATCCTGGACCT-3′. We also tested whether extended CHYSEL sequences, 30 amino acids in total

length from the separation point, might enhance separation by further interacting with the exit tunnel (Luke et al., 2008). We found that these extended viral CHYSEL sequences still created a proportion of fusion product compared with shorter, 19-amino-acid codon-de-optimized CHYSEL sequences (Figure S5C). Mutated PQR sequences that failed to separate were used as linkers for fusion protein experiments. All viral sequences were generated using gene synthesis into a *pUC57* vector (BioBasic) and cloned into *pCAG* for mammalian experiments or *pJFRC7* for *Drosophila melanogaster* experiments. GFP, RFP, and BFP constructs were based on superfolderGFP, TagRFP-T, and mTagBFP2, respectively. SuperfolderGFP and TagRFP-T were chosen for their relatively fast maturation times, 6 min and 100 min, and average turnover rates at 26 hr, respectively (Corish and Tyler-Smith, 1999; Khmelinskii et al., 2012; Pédelacq et al., 2006; Shaner et al., 2008). For GFP and RFP protein concentration and fluorescence intensity measurements, proteins were purified from *E. coli* using GFP-specific chromatography columns (Bio-Rad), and protein concentrations were measured using a Bradford assay with a NanoDrop 2000 (Thermo Fisher Scientific). Samples were serially diluted, and thin samples were imaged on glass slides to reduce any non-linear effects using a standard fluorescence microscope (see "Image Acquisition"). *ShakerGFP* cDNA (R. Blunck, Université de Montréal) and *hs-PER::YFP* (M.W. Young, Rockefeller University) were kind gifts, and all other plasmids were obtained through Addgene. GFP::RFP fusion proteins were verified using immunoblotting (Figure 2), and imaging experiments verified that these large proteins were excluded from the nucleus.

Cell Culture

HEK293, Neuroblastoma-2A (N2A), and 22c10 cells were cultured at 37°C under 5% CO_2 in DMEM (Wisent) and H-Cell (22c10) (Wisent), or for *Drosophila* S2 and Kc cells, at 25°C in Ex-Cell 420 Medium (Sigma-Aldrich). Media for mammalian cells were supplemented with 10% fetal bovine serum (FBS) (Wisent), and 100 U/ml penicillin (Life Technologies) and 100 μg/ml streptomycin (Life Technologies). Cells were transfected with 5 μg of plasmid DNA in 35 mm dishes using Lipofectamine 3000 (Life Technologies). For genome editing experiments, 800 ng of *CRISPR-Cas9* plasmid DNA were co-transfected with 800 ng of repair template circular plasmid in 12-well plates. After 2–7 days, cells were non-enzymatically dissociated and seeded on glass coverslips and prepared for imaging and electrophysiology experiments.

Immunoblotting

Immunoblot experiments were performed four times. One billion cells were placed into lysis buffer (25 mM HEPES, 150 mM NaCl, 1 mM EDTA, and 1% Triton-X) with SIGMAFAST protease inhibitor tablet solution (Sigma-Aldrich). Protein concentrations were measured using a bicinchoninic acid protein assay (Pierce), and 30–40μg of protein was loaded into a NuPAGE Novex 12% Bis-Tris Gel (Life Technologies). Proteins were separated by electrophoresis and transferred to a polyvinylidene fluoride membrane using Invitrogen iBlot dry transfer (Life Technologies). The membrane was blocked in 5% BSA in PBS-T and incubated with the following antibody dilutions: 1:1,000 anti-RFP rabbit polyclonal (R10367, Life Technologies), 1:2,000 anti-GFP rabbit polyclonal (A6455, Life Technologies), and 1:5,000 anti-actin JLA-20 mouse monoclonal (Developmental Studies Hybridoma Bank). Secondary antibodies used were 1:10,000 horseradish peroxidase (HRP)-conjugated donkey anti-rabbit immunoglobulin G (IgG) (Jackson ImmunoResearch Laboratories) and HRP-conjugated goat anti-mouse IgG (Abcam). All antibodies were dissolved in 5% BSA in PBS-T. Membranes were imaged using the Pierce ECL Chemiluminescence Detection Kit for HRP (Thermo Scientific). The ratio of band intensity of GFP or fusion products was normalized to actin and quantified using ImageJ, as described previously (Cvetkovska et al., 2013). We performed western blots on all *PQR* constructs used in experiments and confirmed the absence of fusion protein products for GFP, RFP, ShakerGFP, PER, Cut, and RPL13A proteins (Figures S5 and S6).

Image Acquisition

Fluorescence and bright-field microscopy were performed using a Zeiss AxioScope A1, an Olympus laser scanning confocal microscope FV1000, and a Perkin Elmer UltraView spinning disk confocal Leica DMLFSA microscope. All images were acquired at 512 × 512 pixels using a 40× water objective, numerical aperture (NA) 1.0 (epifluorescence), 60× oil, NA 1.4, or 63× water, NA 0.9 objectives (confocal) corresponding to an 215 × 160-μm or 120 × 110-μm field of view, respectively. Fluorescence emission was detected using a charge-coupled device camera (MRm) for the Zeiss and (OrcaER, Hamamatsu) Leica microscopes and photomultiplier tubes for the Olympus microscope. All image acquisition parameters were fixed for each imaging channel for exposure time, excitation intensity, gain, and voltages. Cells that were dimmer or brighter than the fixed initial acquisition dynamic range were not included for analysis. We verified that shifting the acquisition window across fluorescence intensity ranges produced linear correlations throughout the range. In co-transfection of GFP and RFP experiments, cells that were non-fluorescent in either the green or red channel were not imaged; therefore, the R^2 values for our co-transfection experiments are likely to be overestimates of the true R^2.

Image Analysis

Images were selected for analysis based on identification of single cells and low background. Images were adjusted for contrast and brightness only. Image analysis was performed blind to genotype. Fluorescence pixel intensities were measured in several regions of interest (ROIs) within the cell using a custom written program in MATLAB (MathWorks) or ImageJ. Average pixel intensities were calculated from three ROIs of 10 × 10 pixels for measurements within the cytoplasm and nucleus, or from five ROIs of 3 × 3 pixels for membrane and mitochondrial measurements. For *Drosophila* small lateral ventral neuron analysis, six ROIs of 6 × 6 pixels were measured from six neurons per lobe, and six animals per time point were chosen. All signal intensities were background subtracted from the average of three 10 × 10 ROIs surrounding the cell. We verified that RFP was still cyclically co-translated at later time points by analyzing red fluorescence intensities on days 5 and 6 using a lower acquisition setting (Figure S4C).

Electrophysiology

A standard whole-cell voltage clamp was used to record potassium currents from HEK293 cells. During recordings, cells were maintained for 1–2 hr at 25°C in extracellular solution consisting of 140 mM NaCl, 10 mM $CaCl_2$, 5 mM KCl, 10 mM HEPES, and 10 mM glucose at pH 7.4, 319 mOsm. Patch electrodes were pulled from standard wall borosilicate glass (BF150-86-10, Sutter Instruments) with 3–5 MΩ resistances. The intracellular pipette solution was 150 mM KCl, 2 mM $MgCl_2$, 1 mM $CaCl_2$, 2 mM EGTA, 20 mM HEPES, and 20 mM sucrose at pH 7.23, 326 mOsm. Whole-cell potassium currents were low pass filtered at 5 kHz and measured using an Axopatch 200B amplifier (Axon Instruments) and recorded using a DigiData 1200 with pClamp9 software (Molecular Devices). All pipette and cell capacitances were fully compensated. Cells were held at −80 mV and then given +10 mV steps of 35 ms. The steady-state current elicited at +30 mV was used for analysis. Consistent cell capacitance and membrane and access resistances were verified before and after recordings.

Statistical Analysis

Linear correlations were calculated by fitting the data to a simple linear regression model with the coefficient of determination, R^2. We tested the null hypothesis that the variables were independent of each other and that the true R^2 value was 0. To test the confidence of our R^2 values for each experiment, we calculated the F statistic and its p value of the F-test on the regression model. We also used the permutation test to obtain a p value on the likelihood of obtaining our R^2 value by randomly shuffling the data and calculating a new R^2 value, repeated for one million runs (Figure S1). Both approaches gave similar p values for all experiments.

To compare the R^2 values generated from *PQRs* to other conditions, we used the data from the fusion protein experiments as positive controls. We used the bootstrap method to generate a 95% confidence interval for the true R^2 value of the positive controls. We randomly chose 80% of the positive control data points to calculate a new R^2 value and repeated this for ten million runs, and used these simulated R^2 values to obtain upper and lower estimates of the positive control R^2 values (Figure S1). All statistical analyses were performed using custom-written programs in MATLAB (MathWorks).

Drosophila melanogaster Circadian Experiments

To generate the *UAS–RFP-PQR-PER::YFP* construct, *PER::YFP* was amplified from *hs-PER::YFP*, ligated with the *RFP-PQR* fragment, and inserted into the *pUAST* vector. Transgenic fly lines were created using P-element transgenesis (Bestgene). The *UAS-RFP-PQR-PER::YFP* flies were crossed to the *per-Gal4* driver line, *P{GAL4-per.BS}3*. Crosses were maintained at 25°C in a 12-hr light/dark cycle incubator, and newly eclosed F1 progeny were entrained for 3 days before collection. Six female flies were selected for each time point (6 a.m. and 6 p.m., or zeitgeber time ZT0 and ZT12, respectively). Flies were fixed in 3.7% paraformaldehyde in 0.2 M carbonate-bicarbonate buffer (pH 9.5) at 4°C for 12 hr. Fly brains were then dissected, mounted on slides, and imaged using confocal microscopy.

Drosophila melanogaster Dendritic Complexity Experiments

The *pJFRC-20XUAS-IVS-RFP$_{nls}$-PQR-cut* construct was created by genomic extraction of the *cut* coding region from the fly *UAS-cut* (Grueber et al., 2003). The cDNA was ligated to *RFP$_{nls}$-PQR,* and the resulting construct was cloned into the *pJFRC7* vector. The transgenic fly *w*$^{-}$; P{*20XUAS-IVS-RFP$_{nls}$-PQR-cut}*attP was created by PhiC31 integrase-mediated transgenesis (Bestgene). Homozygous flies *w*$^{-}$; P{*20XUAS-IVS-RFP$_{nls}$-PQR-cut}attP,* were crossed to homozygous *w*$^{-}$*; 221-Gal4, UAS-mCD8::GFP* to selectively express *RFP$_{nls}$-PQR-cut* in class I da neurons. Crosses were maintained at 18°C and wandering third-instar larvae were used for imaging. Larvae were dissected in PBS and the anterior end, gut, tracheal tubes, and fat bodies were removed prior to imaging. Class I ddaE living neurons were imaged using a Fluoview FV1000 confocal laser scanning microscope (Olympus). Neuronal morphology was visualized using the membrane-bound mCD8::GFP, and Cut protein levels were determined by ROI analysis of nuclear red fluorescence intensity. Complete dendritic arbors were reconstructed and the number of terminal branches and total dendritic length were computed using the NeuronJ plugin in Fiji.

Genome Editing Using CRISPR-Cas9

Guide RNAs were designed as 20 bp DNA oligonucleotides and cloned into *pX330* (Addgene, 42230) and co-transfected with a circular *PQR* repair template using Lipofectamine 3000 (Life Technologies). All CRISPR-Cas9 guide RNAs were tested for activity using SURVEYOR Nuclease and SURVEYOR Enhancer S (Transgenomics) on extracted genomic DNA. Re-annealed products were analyzed on 4%–20% Novex TBE polyacrylamide gels (Life Technologies). Repair templates were constructed by placing *PQR-XFP* between homology arms specific to human, mouse, or fly *RPL13A*. The homology arms lacked the *RPL13A* promoter, which prevented expression of the *PQR-XFP* until in-frame genomic integration within an active coding gene. Left and right homology arms were 1.0 kb for the human genome, 1.5 kb for the mouse genome, and 700 bp for the *Drosophila* genome. Cellular fluorescence from *PQRs* was observed four days post-transfection.

Validation of *PQR* Genomic Insertion

Genotyping experiments were performed in experimental duplicate. Integration of *PQR* into the endogenous *RPL13A* or *IgK* genomic locus was validated by genomic DNA extraction 6 days post-transfection and genotyping using primers outside and within the homology arms of the repair template. The 5′ and 3′ ends were probed with two sets of primers, and the endogenous *RPL13a* or *IgK* locus was PCR amplified. Restriction digests were then performed on PCR products at sites specific for *PQR*. All genomes were sequenced to identify the *PQR* and genomic junctions.

To verify that insertion of our *PQR* constructs into the endogenous *RPL13A* locus did not produce fusion protein products, we performed western blots on manually enriched populations of the knockin cell lines (Figure S6). No fusion products were detected, and the enriched populations of knockin cell lines were indistinguishable from wild-type cells with respect to phenotype and growth rate, and have been passaged multiple times. Finally, we also used qPCR to verify that that the genome-edited cells produced RNA transcripts at similar levels to wild-type (Figure S6).

Real-Time qPCR

For relative quantification of *RPL13A* and *IgK* mRNA levels from manually enriched stable cell lines, total RNA was extracted and purified using the PureLink RNA mini kit (Life Technologies) and genomic DNA was eliminated using DNaseI (New England Biolabs). Total RNA was reverse transcribed with gene-specific primer cocktails (2μM final concentration of each primer) using Superscript III reverse polymerase (Life Technologies). This cDNA template was used for real-time PCR using the TaqMan Fast Advanced Mastermix (Life Technologies). Real-time PCR amplification was detected using the StepOnePlus Real-Time PCR System (Applied Biosystems) and cycle quantification values were calculated using StepOne software. Experiments were performed in two to three experimental replicates with two technical replicates. Relative gene expression was determined using a ΔΔCq method. For relative quantification experiments, cycle quantification values were normalized to *GAPDH* in HEK293, N2A, and 22c10 cells.

For absolute quantification of *RPL13A* and *IgK* mRNA levels from single cells, individual cells were imaged in drops of culture media on Teflon-coated glass slides before extraction and purification of total RNA using the TRIzol reagent (Life Technologies). Absolute quantification of *RPL13A* and *IgK* copy numbers was determined using standard curves generated with synthesized oligo standards containing the *RPL13A* and *IgK* target (sequences shown in Table S1). Primers and double-quenched 5′-FAM/ZEN/IowaBlackFQ-3′ probes were purchased from Integrated DNA Technologies. All DNA and primer sequences used are shown in Table S1.

SUPPLEMENTAL INFORMATION

Supplemental Information includes Supplemental Experimental Procedures, six figures, and one table and can be found with this article online at http://dx.doi.org/10.1016/j.celrep.2015.11.048.

AUTHOR CONTRIBUTIONS

B.E.C. designed the experiments and supervised the project. C.-A.L., I.K., F.E., T.-J.L., V.C., and B.E.C. performed experiments and analyzed the data. C.-A.L., I.K., and B.E.C. wrote the manuscript.

ACKNOWLEDGMENTS

The authors thank Peter Mussells Pires, Sondos Zayed, Alexander Greben, Viktoria Stoudenikina, and Haider F. Altimimi for assistance with experiments. This work was supported by a grant from the Natural Sciences and Engineering Research Council of Canada and awards from the Alfred P. Sloan Foundation and The Scottish Rite Charitable Foundation of Canada (to B.E.C.).

Received: February 20, 2015
Revised: September 16, 2015
Accepted: November 13, 2015
Published: December 10, 2015

REFERENCES

Batulan, Z., Haddad, G.A., and Blunck, R. (2010). An intersubunit interaction between S4-S5 linker and S6 is responsible for the slow off-gating component in Shaker K+ channels. J. Biol. Chem. *285*, 14005–14019.

Bradford, M.M. (1976). A rapid and sensitive method for the quantitation of microgram quantities of protein utilizing the principle of protein-dye binding. Anal. Biochem. *72*, 248–254.

Corish, P., and Tyler-Smith, C. (1999). Attenuation of green fluorescent protein half-life in mammalian cells. Protein Eng. *12*, 1035–1040.

Cvetkovska, V., Hibbert, A.D., Emran, F., and Chen, B.E. (2013). Overexpression of Down syndrome cell adhesion molecule impairs precise synaptic targeting. Nat. Neurosci. *16*, 677–682.

de Felipe, P., Luke, G.A., Hughes, L.E., Gani, D., Halpin, C., and Ryan, M.D. (2006). E unum pluribus: multiple proteins from a self-processing polyprotein. Trends Biotechnol. *24*, 68–75.

de Souza, N.F., and Simon, S.M. (2002). Glycosylation affects the rate of traffic of the Shaker potassium channel through the secretory pathway. Biochemistry *41*, 11351–11361.

Diao, F., and White, B.H. (2012). A novel approach for directing transgene expression in Drosophila: T2A-Gal4 in-frame fusion. Genetics *190*, 1139–1144.

Donnelly, M.L., Gani, D., Flint, M., Monaghan, S., and Ryan, M.D. (1997). The cleavage activities of aphthovirus and cardiovirus 2A proteins. J. Gen. Virol. *78*, 13–21.

Donnelly, M.L., Luke, G., Mehrotra, A., Li, X., Hughes, L.E., Gani, D., and Ryan, M.D. (2001). Analysis of the aphthovirus 2A/2B polyprotein 'cleavage' mechanism indicates not a proteolytic reaction, but a novel translational effect: a putative ribosomal 'skip'. J. Gen. Virol. *82*, 1013–1025.

Doronina, V.A., de Felipe, P., Wu, C., Sharma, P., Sachs, M.S., Ryan, M.D., and Brown, J.D. (2008). Dissection of a co-translational nascent chain separation event. Biochem. Soc. Trans. *36*, 712–716.

Fedyukina, D.V., and Cavagnero, S. (2011). Protein folding at the exit tunnel. Annu. Rev. Biophys. *40*, 337–359.

Fujita, S.C., Zipursky, S.L., Benzer, S., Ferrús, A., and Shotwell, S.L. (1982). Monoclonal antibodies against the Drosophila nervous system. Proc. Natl. Acad. Sci. USA *79*, 7929–7933.

Furtado, A., and Henry, R. (2002). Measurement of green fluorescent protein concentration in single cells by image analysis. Anal. Biochem. *310*, 84–92.

Gaj, T., Gersbach, C.A., and Barbas, C.F., 3rd. (2013). ZFN, TALEN, and CRISPR/Cas-based methods for genome engineering. Trends Biotechnol. *31*, 397–405.

Goedhart, J., van Weeren, L., Adjobo-Hermans, M.J., Elzenaar, I., Hink, M.A., and Gadella, T.W., Jr. (2011). Quantitative co-expression of proteins at the single cell level–application to a multimeric FRET sensor. PLoS ONE *6*, e27321.

Grueber, W.B., Jan, L.Y., and Jan, Y.N. (2003). Different levels of the homeodomain protein cut regulate distinct dendrite branching patterns of Drosophila multidendritic neurons. Cell *112*, 805–818.

Hardin, P.E., Hall, J.C., and Rosbash, M. (1990). Feedback of the Drosophila period gene product on circadian cycling of its messenger RNA levels. Nature *343*, 536–540.

Hsu, E., Pulham, N., Rumfelt, L.L., and Flajnik, M.F. (2006). The plasticity of immunoglobulin gene systems in evolution. Immunol. Rev. *210*, 8–26.

Jinek, M., Chylinski, K., Fonfara, I., Hauer, M., Doudna, J.A., and Charpentier, E. (2012). A programmable dual-RNA-guided DNA endonuclease in adaptive bacterial immunity. Science *337*, 816–821.

Jugloff, D.G., Khanna, R., Schlichter, L.C., and Jones, O.T. (2000). Internalization of the Kv1.4 potassium channel is suppressed by clustering interactions with PSD-95. J. Biol. Chem. *275*, 1357–1364.

Khmelinskii, A., Keller, P.J., Bartosik, A., Meurer, M., Barry, J.D., Mardin, B.R., Kaufmann, A., Trautmann, S., Wachsmuth, M., Pereira, G., et al. (2012). Tandem fluorescent protein timers for in vivo analysis of protein dynamics. Nat. Biotechnol. *30*, 708–714.

Kim, J.H., Lee, S.R., Li, L.H., Park, H.J., Park, J.H., Lee, K.Y., Kim, M.K., Shin, B.A., and Choi, S.Y. (2011). High cleavage efficiency of a 2A peptide derived from porcine teschovirus-1 in human cell lines, zebrafish and mice. PLoS ONE *6*, e18556.

Luke, G.A., de Felipe, P., Lukashev, A., Kallioinen, S.E., Bruno, E.A., and Ryan, M.D. (2008). Occurrence, function and evolutionary origins of '2A-like' sequences in virus genomes. J. Gen. Virol. *89*, 1036–1042.

Mane, V.P., Heuer, M.A., Hillyer, P., Navarro, M.B., and Rabin, R.L. (2008). Systematic method for determining an ideal housekeeping gene for real-time PCR analysis. J. Biomol. Tech. *19*, 342–347.

Novoa, E.M., and Ribas de Pouplana, L. (2012). Speeding with control: codon usage, tRNAs, and ribosomes. Trends Genet. *28*, 574–581.

Pédelacq, J.D., Cabantous, S., Tran, T., Terwilliger, T.C., and Waldo, G.S. (2006). Engineering and characterization of a superfolder green fluorescent protein. Nat. Biotechnol. *24*, 79–88.

Renart, J., Reiser, J., and Stark, G.R. (1979). Transfer of proteins from gels to diazobenzyloxymethyl-paper and detection with antisera: a method for studying antibody specificity and antigen structure. Proc. Natl. Acad. Sci. USA *76*, 3116–3120.

Ryan, M.D., Luke, G., Hughes, L.E., Cowton, V.M., Ten Dam, E., Li, X., Donnelly, M.L.L., Mehrotra, A., and Gani, D. (2002). The aphtho- and cardiovirus "primary" 2A/2B polyprotein "cleavage.". In Molecular Biology of Picornaviruses, E.W. Bert and L. Semler, eds. (ASM Press), pp. 213–223.

Schwanhäusser, B., Busse, D., Li, N., Dittmar, G., Schuchhardt, J., Wolf, J., Chen, W., and Selbach, M. (2011). Global quantification of mammalian gene expression control. Nature *473*, 337–342.

Shalek, A.K., Satija, R., Adiconis, X., Gertner, R.S., Gaublomme, J.T., Raychowdhury, R., Schwartz, S., Yosef, N., Malboeuf, C., Lu, D., et al. (2013). Single-cell transcriptomics reveals bimodality in expression and splicing in immune cells. Nature *498*, 236–240.

Shaner, N.C., Lin, M.Z., McKeown, M.R., Steinbach, P.A., Hazelwood, K.L., Davidson, M.W., and Tsien, R.Y. (2008). Improving the photostability of bright monomeric orange and red fluorescent proteins. Nat. Methods *5*, 545–551.

Straub, C., Granger, A.J., Saulnier, J.L., and Sabatini, B.L. (2014). CRISPR/Cas9-mediated gene knock-down in post-mitotic neurons. PLoS ONE *9*, e105584.

Szymczak, A.L., Workman, C.J., Wang, Y., Vignali, K.M., Dilioglou, S., Vanin, E.F., and Vignali, D.A. (2004). Addendum: Correction of multi-gene deficiency in vivo using a single 'self-cleaving' 2A peptide-based retroviral vector. Nat. Biotechnol. *22*, 760.

Tsai, K.W., Tseng, H.C., and Lin, W.C. (2008). Two wobble-splicing events affect ING4 protein subnuclear localization and degradation. Exp. Cell Res. *314*, 3130–3141.

Vogel, C., and Marcotte, E.M. (2012). Insights into the regulation of protein abundance from proteomic and transcriptomic analyses. Nat. Rev. Genet. *13*, 227–232.

Walker, J.M. (2009). The Protein Protocols Handbook, Third Edition (Humana Press).

Yang, S., Cohen, C.J., Peng, P.D., Zhao, Y., Cassard, L., Yu, Z., Zheng, Z., Jones, S., Restifo, N.P., Rosenberg, S.A., and Morgan, R.A. (2008). Development of optimal bicistronic lentiviral vectors facilitates high-level TCR gene expression and robust tumor cell recognition. Gene Ther. *15*, 1411–1423.

Zhao, M.L., Sable, E.O., Iverson, L.E., and Wu, C.F. (1995). Functional expression of Shaker K+ channels in cultured Drosophila "giant" neurons derived from Sh cDNA transformants: distinct properties, distribution, and turnover. J. Neurosci. *15*, 1406–1418.

Zhou, J.H., Zhang, J., Chen, H.T., Ma, L.N., Ding, Y.Z., Pejsak, Z., and Liu, Y.S. (2011). The codon usage model of the context flanking each cleavage site in the polyprotein of foot-and-mouth disease virus. Infect. Genet. Evol. *11*, 1815–1819.

Update

Cell Reports

Volume 26, Issue 11, 12 March 2019, Page 3172

DOI: https://doi.org/10.1016/j.celrep.2019.02.112

OPEN ACCESS
CellPress

Cell Reports
Correction

Quantification of Protein Levels in Single Living Cells

Chiu-An Lo, Ibrahim Kays, Farida Emran, Tsung-Jung Lin, Vedrana Cvetkovska, and Brian Edwin Chen*
*Correspondence: brian.chen@mcgill.ca
https://doi.org/10.1016/j.celrep.2019.02.112

(Cell Reports *13*, 2634–2644; December 22, 2015)

In the originally published version of this article, the DNA sequence reported in the Experimental Procedures for the *PQR* in *Drosophila* cells was the incorrect variant. The correct DNA sequence for the *PQR* in *Drosophila* cells is 5'-GGAAGCGGAGAAGGTCGTGGTAGT CTACTAACGTGTGGTGATGTAGAAGAAAATCCTGGACCT-3'.

The authors regret this error.

